Room-Temperature Micron-Scale Exciton Migration in a Stabilized Emissive Molecular Aggregate

Supporting Information: Room Temperature Micron-Scale Exciton Migration in a Stabilized Emissive Molecular-Aggregate

Justin R. Caram,[†] Sandra Doria,[†] Dorthe M. Eisele,[‡] Francesca S. Freyria,[†] Timothy S. Sinclair,[†] Patrick Rebentrost,[¶] Seth Lloyd,[¶] and Moungi G. Bawendi[*,†]

[†]*Department of Chemistry, Massachusetts Institute of Technology, Cambridge, MA 02139*

[‡]*Department of Chemistry and Biochemistry, Center for Discovery and Innovation, The City College of New York of The City University of New York, 160 Convent Avenue, New York, New York, 10031 USA*

[¶]*Department of Mechanical Engineering, Massachusetts Institute of Technology, Cambridge, MA 02139*

E-mail: mgb@mit.edu

The supplementary information is divided into three sections. In the first section, we elaborate on diffusion mediated exciton-exciton annihilation, its underlying assumptions, and our fitting strategy (figure 3 of the main text). In the second section, we further elaborate on how we measure homogeneous and inhomogeneous linewidths of light harvesting nanotubes (LHNs) using temperature dependent absorption and emission spectroscopy (figures 4a-b of the main text), and discuss other temperature dependent observations of QY, lifetimes and Stokes shifts. In the third section we discuss our approach to using these linewidths and a structural model of LHNS to understand and predict exciton diffusion (figures 4c-f).

Modeling, simulating and measuring exciton-exciton annihilation

In this section we discuss how we use measurements of EEA to estimate exciton diffusion. To begin, we motivate our choice of a one-dimensional random walk. In a condensed phase system, excitons are dephased by interactions with the local environment prior to radiative decay. In a system with little energetic relaxation, this dephasing interaction changes the energy eigenstate of the exciton and moves its center of mass. From linewidth measurements (figures 4a-b and figures S1a-c), we estimate that the time-scale of interactions with the local environment to be $< 1ps$, considerably faster than the time scale where EEA decreases the excited state population (inset of figure 3). Furthermore, exciton delocalization is unlikely to occur over length scales in excess of one micron in any molecular system at room temperature due to homogeneous disorder. We believe that excitons are thus moving their center of mass prior to annihilating. In an energetically unbiased system, each step has equal probability leading to a random walk. As we see little Stokes shift (Figure S1d), or asymmetry in the emission spectrum, we believe it an unbiased random walk model is appropriate.

Analytical model of one dimensional exciton diffusion

In order to model EEA (as shown in figures 2 and 3), we make a few simplifying assumptions. First, because of the large aspect ratio of the LHN tubes, we assert that exciton diffusion over long-ranges is dominated by one-dimensional propagation. Second, we model only two excitons participating in annihilation at any given time. This allows us to map one dimensional EEA onto the scheme for diffusion limited coalescence $\mathrm{A} + \mathrm{A} \longrightarrow \mathrm{A}$, a solved problem in statistical physics.[1–3] Third, we assert that radiative and non-radiative decay rates are not functions of inter-exciton interactions, allowing us to separate their contribution from the annihilation process. Fourth, we assume the excitons move from lattice site to lattice site with a hopping rate = 2D, where D is the diffusion constant, and that hopping has equal probability in both direction. Fifth, we assert that the annihilation process is nearly instantaneous consistent with prior measurements of biexction lifetimes in other molecular

aggregates.[4]

Following Doering,[3] we define the total concentration of excitons as $\eta(t)$, and the probability that the nearest exciton is at a distance x as $p(x,t)$. The annihilation rate equation goes as the diffusion of the joint probability function $\rho = \eta(t)p(x,t)$,

$$\frac{\partial \rho(x,t)}{\partial t} = D\frac{\partial^2 \rho(x,t)}{\partial x^2}. \tag{1}$$

By asserting an initial poissonian random distribution of excitons such that $p(x,0) = \eta_0 e^{-\eta_0 x}$ it can be shown that the rate equation for just annihilation is

$$\frac{d(\eta(t))}{dt} = -\sqrt{\frac{2D}{\pi t}}\eta(t)^2 + O(D)\eta(t)^2. \tag{2}$$

At short times, the first term dominates, while at longer times, the second term leads to an "effective" repulsion between excitons due to the rapid depletion of nearest neighbors.

From this result, we can arrive at the rate equation that is commonly used to fit EEA. Similar to Suna[5] and others,[6–10] we use impulsive excitation by an ultrafast laser to create an initial density η which decays accordingly:

$$\frac{d(\eta(t))}{dt} = -\eta(t)/t_{tot} - \sqrt{\frac{2D}{\pi t}}\eta(t)^2. \tag{3}$$

where D is the diffusion constant, and t_{tot} is the total lifetime of the single exciton (in the absence of annihilation). The analytical solution is as follows:

$$\eta(t) = \frac{2\eta\sqrt{\alpha}e^{-\alpha t}}{2\sqrt{\alpha} + \sqrt{\pi}\beta\eta\mathrm{Erf}[\sqrt{\alpha t}]}. \tag{4}$$

where $\alpha = 1/t_{tot}$, $\beta = \sqrt{2D/\pi}$ and $\mathrm{Erf}(x) = \int_{-\infty}^{x} e^{-x^2}$. We plot the normalized equation in figure 3 for different initial densities. In principle, this equation can be fit directly to the photoluminescence decay to estimate the diffusion coefficient though we employ a slightly

different strategy in the next section.

As a secondary measurement, we use the normalized quantum yield to estimate the diffusion length. The quantum yield is the integrated population divided by the population decay given no EEA.

$$QY(\eta) = \frac{\int_0^\infty \eta(t)dt\Big|_{\eta,\alpha}}{\int_0^\infty \eta e^{-\alpha t}dt} = \frac{\alpha}{\eta}\int_0^\infty \eta(t)dt\Big|_{\eta,\alpha} \tag{5}$$

We numerically integrate equation 4 in MATLAB for each density and fit the relative quantum yield.

Experimental determination of exciton concentration and exciton diffusion distance

To extract exciton diffusion lengths and constants we relate the power of our focused ultrafast excitation to the an initial density of excitons per length of LHN. The energy per pulse χ is measured using a power meter, and the excitation radius (R_b) is the fit half-width-half max of a Gaussian excitation profile measured using a CCD camera. We assume uniform average intensity over that region for simplicity. The initial exciton density is given by equation 1 in the main text. Geometric parameters for the J-Aggregate provided from previous report,[11,12] used to set the lateral displacement per monomer along the primary axis of the nanotube a_0, including both inner and outer walls.

In order to fit equation 4 to the collected data we first fit the long time limit (400-1100 ps) to an exponential decay.

$$\eta_{400-1100ps}(t) = \eta_0 e^{-t/t_{tot}}. \tag{6}$$

and obtain t_{tot}. We then divide the first order kinetics from the measured data and take the reciprocal to obtain a new normalized expression, which describes the exciton annihilation dynamics.

$$\mathrm{EEA}(t) = 1 + \sqrt{\frac{D}{2\alpha}}\eta\mathrm{Erf}[\sqrt{\alpha t}] = 1 + \frac{\bar{x}_{rms}\eta}{4}\mathrm{Erf}[\sqrt{\alpha t}]; \tag{7}$$

We separately measure the instrument response function and fit it to the following equation

$$\mathrm{IRF}(t) = c_1 e^{-t^2/c_2} + \mathrm{Erf}(c_2 t) e^{-c_3 t} \tag{8}$$

We can then fit the collection of photoluminescent decay at a given temperature by taking the numerical convolution of equations 4 and 8 ($\mathrm{EEA}(t) * \mathrm{IRF}(t)$). An example fit is shown in figure 3g of the main text.

Finally, in figure S4, we estimate the effect of a finite size distribution on signatures of exciton-exciton annihilation. Briefly, we estimate the incidence of multiple (> 2) excitations for different initial excitation densities and LHN lengths assuming a Poisson distribution of excitations. Using TEM we find the distribution of aggregate lengths. We observe that at 0.5 excitations per micron, only 20% of excitons are participating in annihilation, assuming the TEM represents an accurate sample of LHN domain sizes.

Fitting absorption and emission to estimate disorder

Temperature dependent absorption was collected at 90 degrees using a Cary UV-Vis spectrometer. Temperature-dependent fluorescence spectra was collected at 45 degrees using 520nm excitation. We correct the fluorescence spectra for sample reabsorption.[13] Both spectra are fit to Voight functions which reflect the convolution of Lorentzian and Gaussian linewidths:

$$Y = \frac{a_0 \int_{-\infty}^{\infty} \frac{\exp(-t^2)}{a_3^2 + (\frac{x-a_1}{a_2} - t)^2} dt}{\int_{-\infty}^{\infty} \frac{\exp(-t^2)}{a_3^2 + t^2} dt} \quad , \tag{9}$$

with a_2 equal to the Gaussian width and a_3 derived from the ratio of Lorentzian and Gaussian components. We take the Gaussian width to represent the static energetic disorder, and the Lorentzian contribution to represent the temperature dependent dynamic fluctuations.[14] For this reason, we fix the Gaussian width for all temperatures and fit only the Lorentzian component, which shows excellent agreement to the data (figure4a). The FWHM reported in

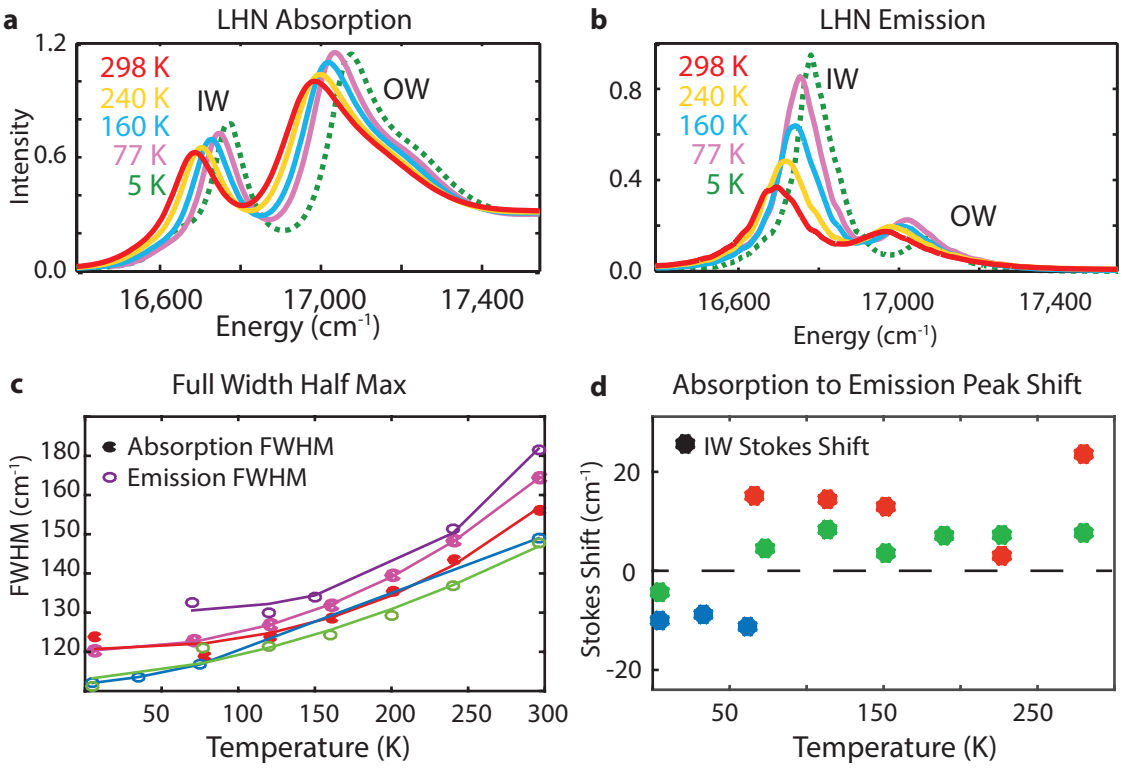

Figure S 1: a, Typical absorption and b, emission spectra from all temperatures. c, Full width half max for 4 sets of temperature dependent experiments (color coded) Trend fit to equation 2. d, Inner wall stokes shift is plotted, and is essentially zero with in the experimental error. Different colors represent different sample preparations.

figure 4b and supplemental figure 1c is calculated using the *modified Whiting* approximation:

$$FWHM = 0.5346\Delta\omega_L + \sqrt{0.2169\Delta\omega_L^2 + \Delta\omega_G^2}, \tag{10}$$

where $\omega_G = 2\sqrt{\ln(2)}|a_2|$ is the Gaussian width and $\omega_L = 2|a_2|a_3$ is the Lorentzian width. Fits are reported tables 1 and 2.

To determine the temperature dependence of the disorder, we fit the observed FWHM as a function of temperature to $\Delta\omega_L(T) = a_H T^n$. We will use this to generalize our model across multiple temperature scales. We plot different experiments supplementary figure 1c. Th excellent agreement of the lorentzian linewidth to a temperature power law strongly suggests that pure dephasing is primarily responsible for the homogeneous linewidth, rather than specific phonon modes.

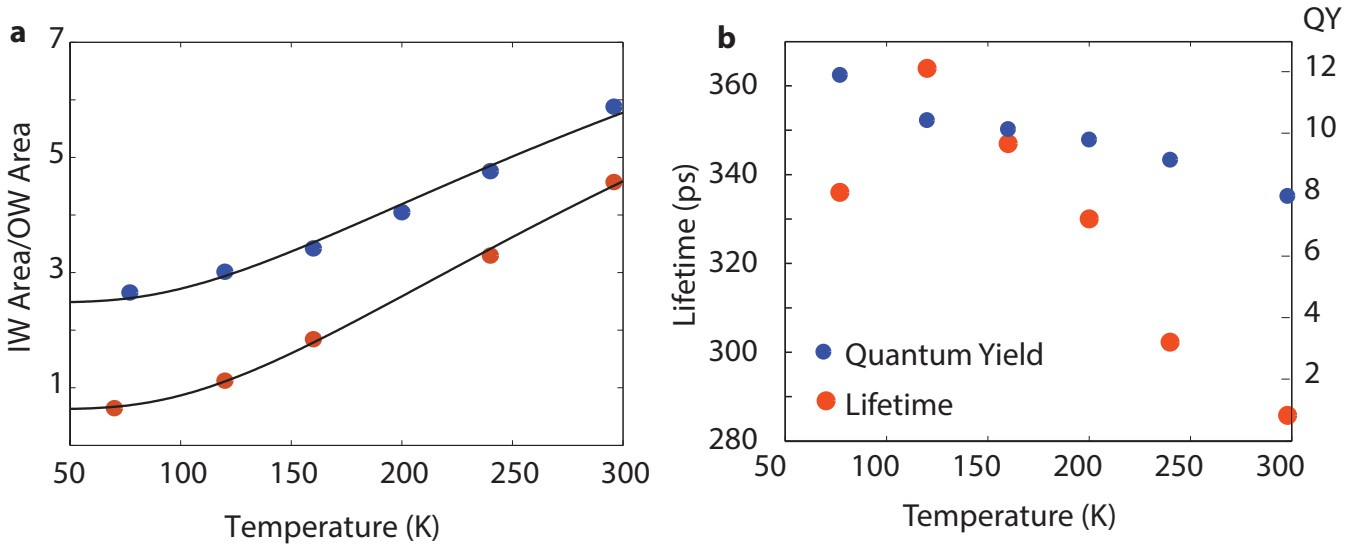

Figure S 2: a) Inner and outer wall peak ratios follow a Boltzmann distribution, suggesting an equilibrium population of inner and outer wall excitons, and weak coupling between each wall. Each color represents a different measurement. b) Lifetime and quantum yield increase slightly as temperature is decreased, likely due to to lower homogeneous disorder.

We also fit the intensity ratio between inner and outer wall emission peaks as a function

of temperature T to a Boltzmann distribution:

$$Y = b_1 + b_2 e^{\frac{-\Delta E}{K_B T}}, \tag{11}$$

where K_B is the Boltzmann constant and ΔE is obtained experimentally by averaging the energy difference between outer and inner wall emission over the different temperatures and b_1 and b_2 are constants. ΔE values and fit parameters are reported in table S3, and plotted in supplemental figure 2a. This demonstrates that the inner and outer walls reach thermal equilibrium prior to emission. In figure 2b we plot the temp-dependent overall quantum yield the lifetimes fit from equation 6. In figure S3 we show the experimental setup used to measure exciton exciton annihilation. We collect PL spectra using and Ocean Optics Spectrometer, or collect PL lifetimes using an avalanche photodiode attached to a time correlated single photon counter.

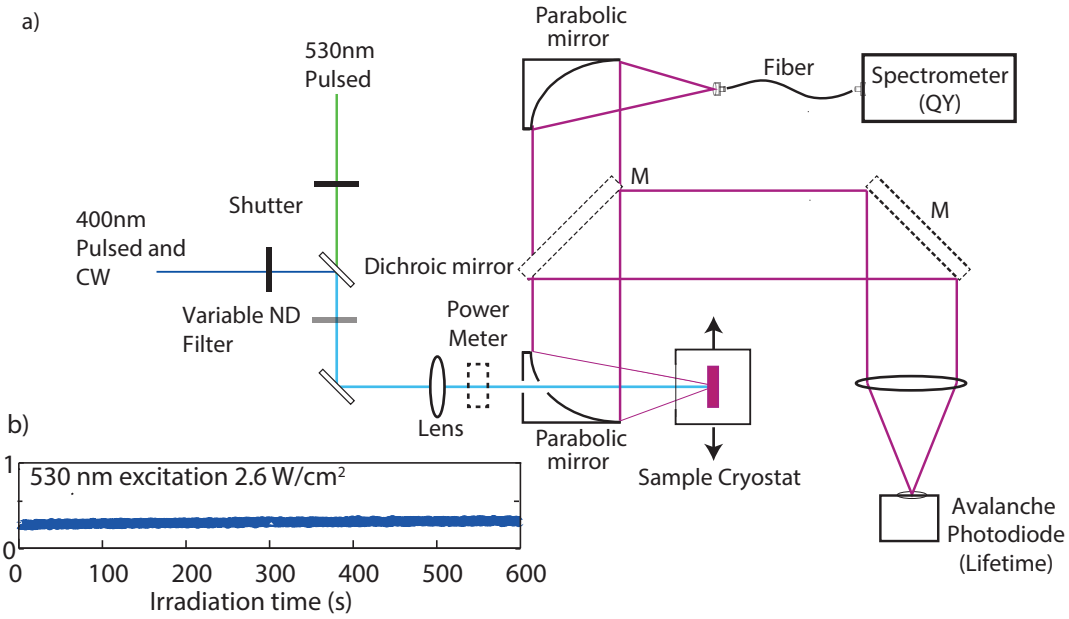

Figure S 3: a) Our experimental setup for studying EEA. We use either 400 or 530nm pulsed or CW excitation, and collect the PL spectra, or time-resolved PL for varying pulse energies. b) We plot the PL intensity under continuous excitation at 530nm, observing no photobleaching for this power.

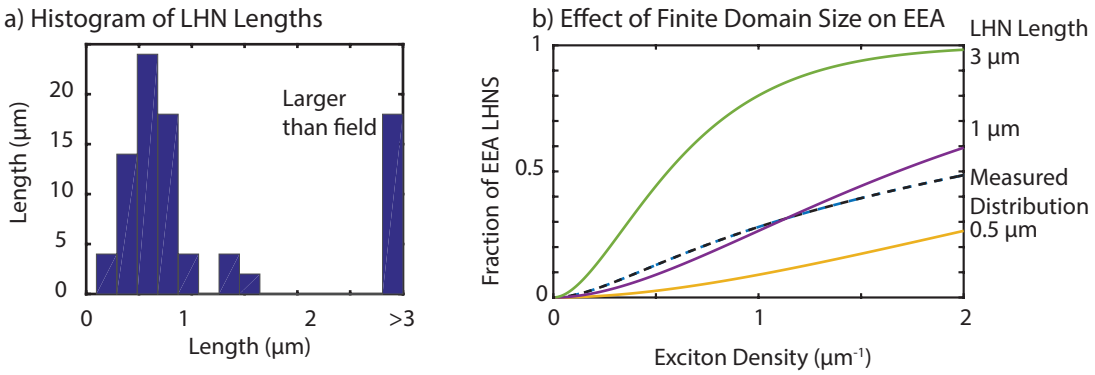

Figure S 4: We estimate the number of aggregates which *can* participate in EEA as a function of excitation density and length of aggregate. From TEM (figure 1d and others), we histogram LHN lengths (in a), with those that extend across the full field binned at 3 μms. In (b) we use a Poisson distribution of excitations to determine the fraction of LHNs that *can* participate in EEA (number of excitons > 0 or 1) for a given exciton density and LHN length. Shorter domain sizes have negligible contribution to the EEA signal. Using the measured distribution in from (a), we find that 20% of excitations can participate in EEA at 0.5 excitations per micron (b) (dotted line). This contributes to the offset in the quantum yield observed in figure 3h

From disorder to exciton diffusion

To relate exciton transport to energetic disorder, we consider a simple model (from reference 15) of a linear chain of sites (molecules) with intersite dipolar coupling energy hJ, and a Gaussian distribution of site energies with a standard deviation of $\hbar\Delta\omega_I$ which we obtain from from the temperature-dependent FWHM fit above ($\omega_I = \Delta\omega_G/2\sqrt{2ln2}$). Starting with an excitation on a single site, it will initially propagate through delocalization (ballistically) with a maximum velocity of $2J$. In the limit of no homogeneous broadening the wavepacket accumulates random net phase due to static disorder in accordance with normally distributed energetic differences between monomers:

$$\Delta\phi = \frac{\Delta\omega_I}{2J}\sqrt{2Jt}, \tag{12}$$

The wavepacket extent is limited by accumulating a net phase of $\phi = \pi$. Solving for t, we find a localization time $t_\ell = 2\pi^2 J/\Delta\omega_i^2$. Introducing homogeneous broadening gives us a competing time scale $t_H = 1/\omega_H$, where $\omega_H = \omega_L/2$ from the previously fit Lorentzian

linewidth. The exciton delocalizes until it reaches its delocalization length ($\ell = 2Jt_\ell$), or it interacts with the environment during t_H. The exciton thus undergoes a random walk in an unbiased energy landscape described by the following equation.

$$\sqrt{\langle \Delta x^2 \rangle} = x_{rms} = \underbrace{S}_{stepsize} \sqrt{\underbrace{t_{tot}/t_H}_{number of steps}}. \tag{13}$$

If the system fully delocalizes before it interacts with the local environment ($t_\ell < t_H$), the step size is fixed to $S_1 = \ell = 2Jt_l = 4\pi^2 J^2/\Delta\omega_i^2$ and $x_{rms1} = 4\pi^2 J^2/\Delta\omega_i^2 \sqrt{t_{tot}/t_H}$. If it instead interacts with the environment before it delocalizes ($t_H < t_\ell$) then $S_2 = 2Jt_H$ and the $x_{rms2} = 2J\sqrt{t_{tot}t_H}$. We use a Monte Carlo diffusion model described in the main text of the paper to a diffusion constant. Briefly, we generate Poisson distributed set of interaction times with the environment (with the characteristic time scale t_H set by the room temperature spectrum). At room temperature, t_H is greater than t_ℓ, the distance stepped so (S_2). The time scale of each step is taken to be t_H. Each trajectory is then re-sampled at even time points, and the endpoints at each time are histogrammed and fit to a Gaussian, which gives the RMS diffusion at each step. The square of this is fit to a line to determine the diffusion constant.

We determine the lateral displacement per unit step of exciton propagation using a previously characterized Frenkel exciton Hamiltonian for the inner wall of LHNs[16–18] In this model, each C8S3 monomers has a transition frequency drawn from a Gaussian distribution centered at 18,868 cm^{-1} ± 600 cm^{-1}, corresponding to a monomer absorption wavelength of ∼530 nm. The coupling (off-diagonal elements of the Hamiltonian) is determined using the extended dipole approximation. The charges on each aggregate are 0.34e with a distance separation of 0.7 nm as in previous work.[12] The aggregate geometry is constructed following reference 17. Briefly, the inner wall of the aggregate consists of six intertwined helices of radius 5.455 nm. In the helix, each subsequent molecule is 0.04668 nm displaced down the primary axis of the LHN (z-axis), and rotated 8.6° about the z-axis. The transition dipole

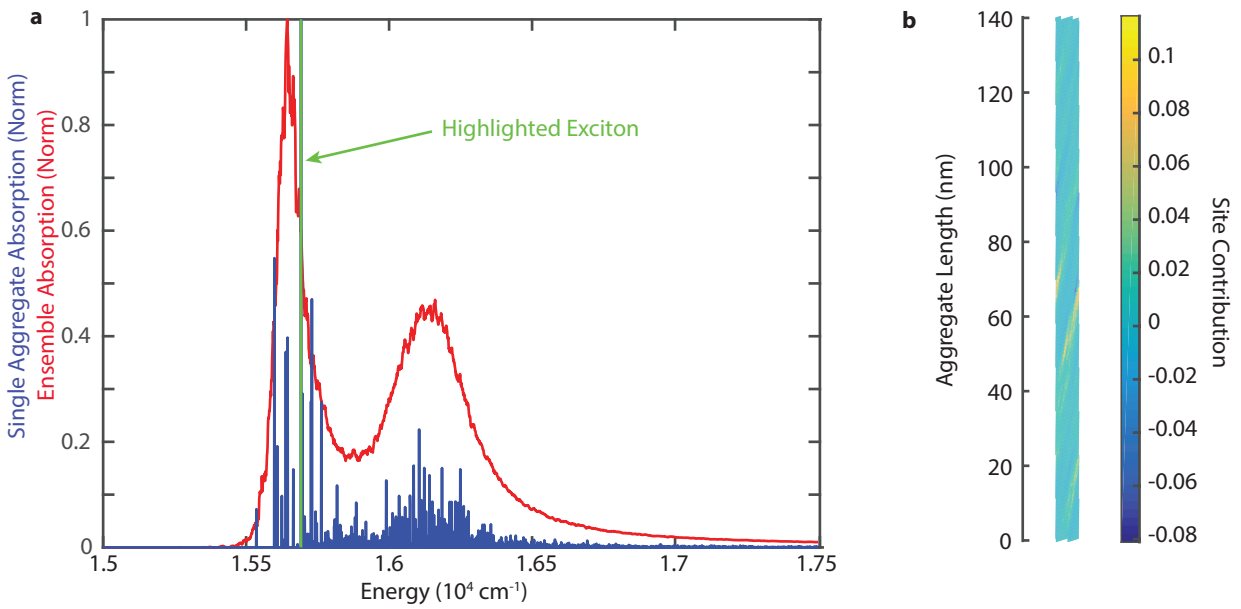

Figure S 5: a) In blue we plot the stick spectrum of the dipole weighted eigenvalues of a single aggregate Hamiltonian with 600 cm^{-1} of diagonal disorder. In red, we plot the ensemble average of 300 different realizations of this Hamiltonian. b) The exciton wavefunction is plotted for the highlighted eigenvalue in part a. The direction of strongest delocalization is helical along the aggregate.

Table S 1: Fit Parameters obtained with the model in eq. 9 (fixed gaussian width) for the absorption spectra

First run

Temperatures	Height	Center (cm^{-1})	ω_L (cm^{-1})	ω_G (cm^{-1})
5K	0.2354 ± 0.0003	16756.1 ± 0.2	67 ± 2	79 ± 2
70K	0.2307 ± 0.0007	16747.8 ± 0.3	74 ± 2	79 ± 2
120K	0.2205 ± 0.0003	16731.7 ± 0.2	74 ± 3	79 ± 2
160K	0.2126 ± 0.0003	16715.0 ± 0.2	80 ± 2	79 ± 2
200K	0.2056 ± 0.0003	16696.7 ± 0.2	89 ± 1	79 ± 2
240K	0.1957 ± 0.0003	16676.4 ± 0.2	100 ± 2	79 ± 2
296K (R.T.)	0.1780 ± 0.0004	16650.7 ± 0.6	110 ± 3	79 ± 2

Second run

Temperatures	Height	Center (cm^{-1})	ω_L (cm^{-1})	ω_G (cm^{-1})
70K	0.449 ± 0.002	16786.5 ± 0.2	105 ± 15	44 ± 8
120K	0.433 ± 0.001	16774.2 ± 0.2	107 ± 12	44 ± 8
160K	0.413 ± 0.002	16756.5 ± 0.2	114 ± 18	44 ± 8
200K	0.379 ± 0.003	16733.2 ± 0.5	121 ± 17	44 ± 8
240K	0.355 ± 0.004	16712.4 ± 0.9	141 ± 10	44 ± 8
296K (R.T.)	0.318 ± 0.009	16692.1 ± 0.9	149 ± 15	44 ± 8

Third run

Temperatures	Heigth	Center (cm^{-1})	ω_L (cm^{-1})	ω_G (cm^{-1})
77K	0.701 ± 0.002	16748.8 ± 0.4	102 ± 5	49 ± 5
120K	0.696 ± 0.002	16742.3 ± 0.3	107 ± 8	49 ± 5
160K	0.675 ± 0.002	16729.1 ± 0.3	111 ± 9	49 ± 5
200K	0.656 ± 0.002	16717.4 ± 0.3	114 ± 11	49 ± 5
240K	0.639 ± 0.002	16704.7 ± 0.2	121 ± 10	49 ± 5
296K (R.T.)	0.617 ± 0.002	16687.6 ± 0.3	131 ± 13	49 ± 5

Table S 2: Fit parameters obtained with the model in eq. 9 (fixed gaussian width) for emission spectra

1	Inner wall							
T	Height (x 10^{11})	Center (cm^{-1})	ω_L (cm^{-1})	ω_G (cm^{-1})				
5K	2.331 ± 0.002	16764.80 ± 0.07	37 ± 1	91.0 ± 0.2				
35K	2.182 ± 0.002	16763.40 ± 0.07	38 ± 2	91.0 ± 0.2				
65K	1.852 ± 0.002	16758.90 ± 0.08	43.0 ± 0.9	91.0 ± 0.2				
296K	1.031 ± 0.002	16680.1 ± 0.1	86 ± 1	91.0 ± 0.2				
2	Inner wall				Outer wall			
T	Height (x 10^{12})	Center (cm^{-1})	ω_L (cm^{-1})	ω_G (cm^{-1})	Height (x 10^{12})	Center (cm^{-1})	ω_L (cm^{-1})	ω_G (cm^{-1})
70K	9.43 ± 0.04	16767.3 ± 0.3	95 ± 8	68.0 ± 0.6	0.902 ± 0.005	17071 ± 3	$10^{-5} \pm 10^{-6}$	120.0 ± 3
120K	6.11 ± 0.05	16752.6 ± 0.3	92 ± 6	68.0 ± 0.6	0.919 ± 0.004	17057 ± 1	8.7 ± 2	120.0 ± 3
160K	4.95 ± 0.02	16736.3 ± 0.2	97 ± 9	68.0 ± 0.6	0.996 ± 0.004	17044 ± 1	42 ± 4	120.0 ± 3
200K	3.83 ± 0.02	16693.6 ± 0.2	118 ± 12	68.0 ± 0.6	1.140 ± 0.003	17010.3 ± 0.9	100 ± 9	120.0 ± 3
296K	2.500 ± 0.007	16663.6 ± 0.2	142 ± 15	68.0 ± 0.6	0.994 ± 0.003	16984.7 ± 0.7	136 ± 10	120.0 ± 3
3	Inner wall				Outer wall			
T	Height (x 10^{12})	Center (cm^{-1})	ω_L (cm^{-1})	ω_G (cm^{-1})	Height (x 10^{12})	Center (cm^{-1})	ω_L (cm^{-1})	ω_G (cm^{-1})
70K	2.517 ± 0.004	16738.00 ± 0.05	78 ± 1	63.1 ± 0.9	0.551 ± 0.003	17018.4 ± 0.3	84 ± 5	93 ± 4
120K	2.145 ± 0.009	16733.60 ± 0.05	79.4 ± 0.7	63.1 ± 0.9	0.503 ± 0.007	$17012.6 + \pm 0.2$	94 ± 4	93 ± 4
160K	1.982 ± 0.009	16724.70 ± 0.05	82 ± 1	63.1 ± 0.9	0.504 ± 0.007	17002.9 ± 0.2	106 ± 6	93 ± 4
200K	1.725 ± 0.001	16712.60 ± 0.06	879.3 ± 0.8	63.1 ± 0.9	0.504 ± 0.008	16992.6 ± 0.2	119 ± 5	93 ± 4
240K	1.428 ± 0.001	16697.90 ± 0.07	97.2 ± 0.8	63.1 ± 0.9	0.485 ± 0.009	16980.8 ± 0.2	134 ± 5	93 ± 4
296K	1.042 ± 0.001	16675.50 ± 0.08	113.2 ± 0.9	63.1 ± 0.9	0.431 ± 0.001	16963.3 ± 0.2	158 ± 7	93 ± 4

Table S 3: Fit Parameters from eq. 11 in two different (1 and 2) temperature dependent experiments.

Parameters	1	2
$\Delta E(cm^{-1})$	293.5	274.8
b_1	0.129 ± 0.003	0.23 ± 0.01
b_2	1.29 ± 0.01	0.78 ± 0.02

of each molecule is taken to be 47.4° from the axis of the tube and locally tangent to the tube. We found that the strongest coupling of the monomers is in the pointing direction of the dipole as shown in prior reports.[18] We find that exciton delocalization proceeds along the direction of highest coupling (see figure 4). In figure S3 we use this model to simulate an absorption spectrum of a single aggregate, plotting a delta function at the energy of each exciton, with a height equal to the (square) of the excitons total dipole. For the total absorption we simulate the spectrum of an ensemble of aggregates, averaging the dipole weighted excitons for different realizations of disorder. In figure 4c we plot the exciton with the participating dipoles colored according to the contribution of each monomer to the total wavefunction.

References

(1) Simon, H. *J. Phys. A. Math. Gen.* **1995**, *28*, 6585.

(2) Alemany, P. A.; Ben-Avraham, D. *Phys. Lett. A* **1995**, *206*, 18–25.

(3) Ben-Avraham, D.; Burschka, M. A.; Doering, C. R. *J. Stat. Phys. 60*, 695–728.

(4) Dawlaty, J. M.; Bennett, D. I. G.; Huxter, V. M.; Fleming, G. R. *J. Chem. Phys.* **2011**, *135*.

(5) Suna, A. *Phys. Rev. B* **1970**, *1*, 1716–1739.

(6) Paillotin, G.; Swenberg, C. E.; Breton, J.; Geacintov, N. E. *Biophys. J.* **1979**, *25*, 513–533.

(7) Scheblykin, I.; Varnavsky, O.; Bataiev, M.; Sliusarenko, O.; Van der Auweraer, M.; Vitukhnovsky, A. Non-coherent exciton migration in J-aggregates of the dye THIATS: excitonexciton annihilation and fluorescence depolarization. 1998.

(8) Malyshev, V.; Glaeske, H.; Feller, K.-H. Excitonexciton annihilation in linear molecular aggregates at low temperature. 1999.

(9) Valkunas, L.; Ma, Y. Z.; Fleming, G. R. *Phys. Rev. B - Condens. Matter Mater. Phys.* **2006**, *73*.

(10) Engel, E.; Leo, K.; Hoffmann, M. *Chemical Physics* **2006**, *325*, 170–177.

(11) Eisele, D. M.; Cone, C. W.; Bloemsma, E. A.; Vlaming, S. M.; van der Kwaak, C. G. F.; Silbey, R. J.; Bawendi, M. G.; KnoesterJ,; Rabe, J. P.; Vanden Bout, D. A. *Nat Chem* **2012**, *4*, 655–662.

(12) Didraga, C.; Pugžlys, A.; Hania, P. R.; von Berlepsch, H.; Duppen, K.; Knoester, J. *J. Phys. Chem. B* **2004**, *108*, 14976–14985.

(13) Grzywacz, J. *Journal of Luminescence* **1971**, *4*, 244–248.

(14) Mukamel, S. *Oxford Ser. Opt. Imaging Sci.*; Oxford: London, 1999.

(15) Lloyd, S.; Mohseni, M.; Shabani, A.; Rabitz, H. *arXiv preprint arXiv:1111.4982* **2011**,

(16) Didraga, C.; Klugkist, J. A.; Knoester, J. *J. Phys. Chem. B* **2002**, *106*, 11474–11486.

(17) Didraga, C.; Knoester, J. *J. Chem. Phys.* **2004**, *121*, 10687–10698.

(18) Prokhorenko, V.; Steensgaard, D.; Holzwarth, A. *Biophys. J.* **2003**, *85*, 3173–3186.